RSC Advances

ROYAL SOCIETY OF CHEMISTRY

www.rsc.org/advances

Solution-processed indium-zinc-oxide thin-film transistors based on anodized aluminum oxide gate insulator modified with zirconium oxide

Yuzhi Li, Linfeng Lan,* Peng Xiao, Zhenguo Lin, Sheng Sun, Wei Song, Erlong Song, Peixiong Gao, Dan Wang,* Honglong Ning, and Junbiao Peng*

State Key Laboratory of Luminescent Materials and Devices, South China University of Technology, Guangzhou 510640, China

Solution-processed indium-zinc-oxide (IZO) thin-film transistors (TFTs) based on anodized aluminum oxide gate insulator modified with a zirconium oxide (ZrO_x) interlayer were fabricated. By introduction of the ZrO_x interlayer, the IZO-TFTs exhibited improved performance with a higher mobility of 7.8 cm^2 V^{-1} s^{-1}, a lower V_{th} of 4.6 V and a lower *SS* of 0.21 V/dec compared to those without ZrO_x interlayer. Comprehensive studies showed that the Al element easily diffuse into IZO film and formed AlO_x clusters which acted as defects to deteriorate TFT performance; and after modified with a ZrO_x interlayer, the diffusion of Al was suppressed and the Zr diffusing effect almost could be ignored. These results suggested that the introduction of an interlayer with less diffusing effect as well as having an effect of blocking the elements from gate insulator diffusing into the channel layer could be an effective way to improve the electrical performance for solution-processed oxide TFTs.

1. Introduction

Thin-film transistors (TFTs) based on amorphous oxide semiconductors (AOSs), as a promising candidate for unit pixel drivers in active-matrix organic light-emitting diode displays (AMOLEDs) and liquid-crystal displays (LCDs), have attracted a great amount of attention for its competitive performances, including high field-effect mobility, good optical transparency and good processing compatibility with TFT production line using conventional amorphous Si (a-Si) as channel material.[1,2] Over the last decade, a lot of excellent-performance AOSs, such as indium-gallium-zinc oxide (IGZO), indium-zinc oxide (IZO), zinc-tin oxide (ZTO), and indium-zinc-tin oxide (IZTO), have been reported and intensively studied.[3-7] Although the intrinsic property and quality of AOS thin films are the most important factors determined electrical properties of TFTs, the gate insulators also play an important role due to the interface coupling between the gate insulator and the AOS.[8,9] In our previous reports, the high performance IGZO- and IZO-TFTs were successfully fabricated using anodized AlO_x to replace SiO_2 as insulators.[10-12] The low leakage current and relatively high dielectric constant make the anodized AlO_x attractive for the gate insulators of the TFTs. However, the AOS thin films were manufactured by vacuum-based method, which is a major obstacle for further cutting down the fabricated cost. Instead, solution-processed AOS-TFTs are more attractive because of the low-cost and large-area process.[13-16]

Herein, solution-processed IZO-TFTs with anodized AlO_x gate insulator were fabricated. The surface of the anodized AlO_x was modified with a thin solution-processed ZrO_x interlayer. The IZO-TFTs with ZrO_x/AlO_x gate insulator show improved performance compared with IZO-

TFTs with AlO_x gate insulator. The mechanisms for the performance improvement were studied in detailed.

2. Experiments and characterization

To prepare the ZrO_x precursor solution, 0.2 M zirconium oxychloride hydrate ($ZrOCl_2 \cdot 8H_2O$) and 0.5 mL aqueous hydrogen peroxide solution (30 wt%) were added into 4.5 mL 2-methoxyethanol. The solution was stirred vigorously for 4 h to form a transparent solution. For IZO precursor solution, 0.1 M metal precursor solution was prepared by adding indium nitrate hydrate [$In(NO_3)_3 \cdot 4.5H_2O$] and zinc nitrate hydrate [$Zn(CH_3COO)_2 \cdot 2H_2O$] into 2-methoxyethanol with molar ratio of3:2. The solution was stirred at 60 °C for 12 h. Meanwhile, a small amount of monoethanolamine was added to the mixture as stabilizer after the dissolution of the metal salts. Both solutions were filtered through a 0.22 μm syringe filter before spin-coating.

The IZO-TFTs based on ZrO_x/AlO_x bilayer insulator were prepared with the bottom-gate, top-contact configuration, as shown in Fig. 1(a). An aluminium gate electrode was firstly deposited on a glass with a thickness of 300 nm. Then, a 190 nm thick anodic AlO_x layer was formed on the surface of the gate electrode by anodic oxidation technology. The details of anodic oxidation process have ever been reported elsewhere.[10] Then, the ZrO_x precursor solution was spin-coated at 3000 rpm for 30 s on anodic AlO_x layers that were treated by oxygen plasma for 20 min. The ZrO_x thin films were firstly soft-baked at 200 °C for 5 min and then hard-baked at 350 °C for 2 h under ambient condition. The IZO precursor solution was spin-coated on ZrO_x at 3000 rpm for 30 s in air. To minimize fringing current effects and gate leakage, the IZO layer was patterned by removing the films outside the channel area with a mechanically-controlled probe tip. This tip was dragged around each transistor, as close as possible to the channel area, prior to the annealing process.[17] After that, the IZO thin film wasannealed at 120 °C for 10 min

and then annealed at 350 °C for 1 h under air atmosphere. Aluminum thin films (250 nm of thickness), as source and drain electrodes (S/D), were finally deposited on IZO layers by thermal evaporation and patterned using a metal shadow mask. The width (*W*) and length (*L*) of the channel was 1000 μm and 300 μm, respectively. For the IZO-TFTs based on anodic AlO_x signal layer insulators, the IZO thin films were directly spin-coated on the anodic AlO_x layers without ZrO_x layers, and other processes were all the same as those based on anodic ZrO_x/AlO_x bilayer insulators.

X-ray photoelectron spectroscopy (XPS, Kratos, Axis Ultra DLD) using monochromatic Al Kα radiation (~1486.6 eV) was used to examine chemical composition of the oxide films. The XPS data were calibrated with C 1s peak at ~284.6 eV. The thickness and structure of the oxide thin films were characterized by transmission electron microscopy (TEM, FEI Titan Themis 200) equipped with an energy dispersive X-ray spectrometer (EDS). The electrical measurements were performed using a semiconductor parameter analyzer (Agilent 4155C) in air.

3. Results and discussion

Fig. 1(b) and (c) display scanning transmission electron microscopy (STEM) image of the $IZO/ZrO_x/AlO_x/Al$ cross-sectional structure and high-resolution transmission electron microscopy (HR-TEM) image of $IZO/ZrO_x/AlO_x$ cross-section, respectively. Both images reveal a uniform and continuous ZrO_x/AlO_x interface without pinholes or hillocks. The thicknesses of Al, AlO_x, ZrO_x, and IZO were measured to be 130, 190, 14, and 8 nm, respectively, which were closed to those measured with ellipsometer or step profiler. Fig. 1(d) shows the fast Fourier transform (FFT) patterns for different areas indicated in Fig. 1(c), revealing the presence of nanocrystalline IZO, ZrO_x, and AlO_x domains, and the ZrO_x layer had the highest crystallinity.

Fig. 2(b) and (c) show the output characteristics obtained from IZO-TFTs with and without ZrO_x interlayer, respectively. It could be seen clearly that both TFTs showed typical n-channel, saturated characteristics, and the IZO-TFT with ZrO_x interlayer had higher output drain current (I_D). There were no current crowding effects in the low drain voltage (V_D) regimes, indicating that both devices had good contacts between S/D and channel layer. Fig. 2(c) shows the transfer characteristics and the corresponding gate leakage current (I_G) versus gate voltage (V_G) of the IZO-TFTs with and without ZrO_x interlayer. The IZO-TFT without ZrO_x interlayer exhibited a field-effect mobility (μ) of 2.8 $cm^2\ V^{-1}\ s^{-1}$, a threshold voltage (V_{th}) of 4.9 V and a sub-threshold slope (SS) of 0.33 V/dec, while the IZO-TFT with ZrO_x interlayer showed a much better performance with a higher μ of 7.8 $cm^2\ V^{-1}\ s^{-1}$, a lower V_{th} of 4.6 V and a lower SS of 0.21 V/dec. The I_G-V_G curves showed that the leakage current reduced slightly after inserted with ZrO_x layer. The electrical properties of both devices are summarized in Table 1. It was worth noting that the hysteresis of the transfer curves between forward and reverse sweeps was reduced for IZO-TFTs with ZrO_x interlayer, suggesting that there are fewer shallow traps which can be trapped or release under positive or negative gate voltage. To evaluate the total trap density (N_t), including the semiconductor bulk (N_b) and semiconductor/insulator interfacial traps (D_i), N_t was calculated from the SS values,[18]

$$SS = \frac{k_B T}{q}\left[1 + \frac{q^2 N_t}{C_i}\right]\ln 10, \qquad (1)$$

$$N_t = D_i + tN_b, \qquad (2)$$

where q is the elementary electron charge, k_B is Boltzmann's constant, T is the absolute temperature, t is the thickness of channel layer, and C_i is the unit-area capacitance of the insulator. The unit-area capacitance of AlO_x and ZrO_x/AlO_x insulators was 38 nF/cm^2 and 36

nF/cm^2, respectively. N_t of IZO-TFT with ZrO_x interlayer was calculated to be 5.9×10^{11} eV^{-1} cm^{-2}, while the other without ZrO_x interlayer was 1.1×10^{12} eV^{-1} cm^{-2}. The result means that the ZrO_x interlayer has an effect of lowering total trap density. Generally, the smooth surface of the insulator is beneficial for TFT performance.[19,20] To study whether the surface roughness was a major factor influencing the TFTs performance, the root-mean-square (RMS) roughness was obtained from atomic force microscopy analysis (AFM, not shown here). The RMS values of AlO_x and ZrO_x/AlO_x films are 1.98 and 1.46 nm. Although the RMS roughness of ZrO_x/AlO_x film was slightly lower than that of the AlO_x film, it would not be the main factor for the enhanced performance of IZO-TFTs.

To investigate how the ZrO_x interlayer affect the total traps, the samples were characterized by high-angle annular dark-field (HAADF) STEM and EDS. Fig. 3 shows the maps of the elemental distribution of IZO/AlO_x/Al/Glass and IZO/ZrO_x/AlO_x/Al/Glass, respectively, revealing good consistency with the STEM images and uniform distributions for all the elements in each layer. It can be seen clearly that there were Al elements distributing in the whole IZO film for the sample without ZrO_x interlayer, while much fewer Al elements were found in the IZO film for the sample with ZrO_x interlayer. Therefore, the ZrO_x interlayer has an effect of blocking Al elements from diffusing into IZO film, which was supported by the quantitative cross-sectional line scan analysis as shown in Fig. 4. Because the radius of Al^{3+} is 0.053 nm,[21] much smaller than those of In^{3+} (0.080 nm) and Zn^{2+} (0.074 nm),[22] Al element are easy to diffuse in the IZO lattices as interstitials or as AlO_x clusters. Therefore, Al element in the IZO serve as defects which can reduce the carrier mobility.[23] On the other hand, the radius of Zr^{4+} (0.084 nm) is much larger than that of Al^{3+},[24] and it is more difficult for Zr element to diffuse into the IZO film than for Al element, which can be seen clearly in Fig. 4.

To further investigate the effect of diffusing Al in the IZO films, XPS experiments were performed. Four samples—AlO_x/Al/Glass, IZO/AlO_x/Al/Glass, ZrO_x/AlO_x/Al/Glass, and IZO/ZrO_x/AlO_x/Al/Glass—were prepared. Fig. 5(a) and (b) show the O 1s spectra obtained from IZO thin film deposited on AlO_x and ZrO_x/AlO_x, respectively. It was known that the main peak located around 529.7 eV (Peak 1) is related to the oxygen in stoichiometric of the IZO films; the peak at 531.0 eV (Peak 2) is attributed to oxygen vacancies; and the peak located at 532.0 eV (Peak 3) is related to the loosely bound oxygen impurities.[25,26] However, it should be noted that the oxygen vacancies herein cannot be characterized by the O 1s spectra, because the peaks attributed to oxygen vacancies and Al-O bond (seen in Fig. 5(c)) are almost at the same position. The higher relative intensity of Peak 2 of the IZO film on bare AlO_x compared with that of IZO on ZrO_x/AlO_x (seen in Fig. 5(a)) was partly ascribed to Al-O bond in the IZO film. Fig. 5(d) and (e) show the Al 2p and In 3d spectra, respectively, for different samples. The Al 2p peak positions for AlO_x/Al/Glass and IZO/AlO_x/Al/Glass samples were both at 74.45 eV, which was corresponding to AlO_x, supporting that the chemical state of the diffusing Al was the same with that of the anodic AlO_x gate insulator. Furthermore, no Al 2p characteristic peak was found in ZrO_x/AlO_x/Al/Glass and IZO/ZrO_x/AlO_x/Al/Glass samples, which indicated the amount of Al element diffusion observed in the Fig. 4(b) could be ignored. In Fig. 5(e), almost no shifts were found for In 3d peaks for the samples with and without ZrO_x interlayer, indicating that the chemical states of In were not affected by Al diffusion.[22] All these supported that the Al element would only physical diffuse into IZO films on AlO_x signal layer as AlO_x clusters which acted as impurities in the IZO film, While introduced a ZrO_x interlayer remarkably reduce the Al impurities in the IZO films.

Based on these early results and the direct evidence presented here, it can be argued that the enhanced performance obtained in our IZO-TFTs with ZrO_x interlayer is attributed to the reduction of the Al diffusion which acts as impurities and the low diffusion effect of the ZrO_x itself. Therefore, it can be deduced that introducing an interlayer with low diffusion into the channel layer and having an effect of blocking the elements from gate insulator diffusing into the channel layer is an effective way to improve the performance of the oxide TFTs. To the best of our knowledge, it is for the first time to investigate the insulator-semiconductor diffusion effect of the solution-processed TFTs.

4. Conclusions

In summary, solution-processed IZO-TFTs based on anodized AlO_x insulator were fabricated. The IZO-TFTs without ZrO_x interlayer showed poor performance with a mobility of only 2.8 $cm^2\ V^{-1}\ s^{-1}$, a V_{th} of 4.9 V and a *SS* of 0.33 V/dec. By surface modification with the ZrO_x interface, the IZO-TFTs exhibited improved performance with a higher mobility of 7.8 $cm^2\ V^{-1}\ s^{-1}$, a lower V_{th} of 4.6 V and a lower *SS* of 0.21 V/dec. It was supported that the Al element easily diffuse into IZO film and formed AlO_x clusters which acted as defects to deteriorate IZO-TFTs electrical properties. By introducing a ZrO_x interlayer, the diffusion of Al element was suppressed and the Zr diffusing effect almost could be ignored, both of which reduced the defects in the IZO film and improved the IZO-TFTs performance. Our results suggested that the introduction of an interlayer with less diffusing effect could be an effective way to improve active layer quality and lead to higher electrical performance for solution-processed TFTs.

Corresponding author

*Linfeng Lan: lanlinfeng@scut.edu.cn, Dan Wang: wangdan@scut.edu.cn, Junbiao Peng: psjbpeng@scut.edu.cn

Author contributions

The manuscript was written through contributions of all authors. All authors have given approval to the final version of the manuscript.

Acknowledgements

The authors are grateful to the National "863" Project of China (Grant No. 2014AA033002), the National "973" Project of China (Grant No. 2015CB655000), the National Natural Science Foundation of China (Grant Nos. 61204087, 51173049, U0634003, 21225418, and 60937001), the Pearl River S&T Nova Program of Guangzhou (Grant No. 2014J2200053), the Guangdong Province Science and Technology Plan (Grant No. 2013B010403004), the Fundamental Research Funds for the Central Universities (Grant No. 2014ZM0003, and 2014ZZ0028), the National Laboratory for Infrared Physics Open Project (M201406), and the Guangdong Innovative Research Team Program (No. 201101C0105067115).

References

1 K. Nomura, H. Ohta, A. Takagi, T. Kamiya, M. Hirano and H. Hosono, *Nature*, 2004, **432**, 488. 2 E. Fortunato, P. Barquinha and R. Martins, *Adv. Mater.*, 2012, **24**, 2945.

3 H. Yabuta, M. Sano, K. Abe, T. Aiba, T. Den, H. Kumomi, K. Nomura, T. Kamiya and H. Hosono, *Appl. Phys. Lett.*, 2006, **89**, 112123.

4 J. H. Park, Y. B. Yoo, K. H. Lee, W. S. Jang, J. Y. Oh, S. S. Chae and H. K. Baik, *ACS Appl. Mater. Interfaces,* 2013, **5**, 410.

5 H. Q. Chiang, J. F. Wager, R. L. Hoffman, J. Jeong and D. A. Keszler, *Appl. Phys. Lett.*, 2005, **86**, 13503.

6 M. Kim, H. S. Kim, Y. Ha, J. He, M. G. Kanatzidis, A. Facchetti and T. J. Marks, *J. Am. Chem. Soc.*, 2010, **132**, 10352.

7 W. Yang, K. Song, Y. Jung, S. Jeong and J. Moon, *J. Mater Chem. C*, 2013, **1**, 4275.

8 W. Xu, H. Wang, L. Ye and J. Xu, *J. Mater. Chem. C*, 2014, **2**, 5389.

9 J. Ko, J. Kim, S. Y. Park, E. Lee, K. Kim, K. Lim and Y. S. Kim, *J. Mater. Chem. C*, 2014, **2**, 1050.

10 L. Lan and J. Peng, *IEEE Tran. Electr. Devices*, 2011, **58**, 1452.

11 L. Lan, M. Zhao, N. Xiong, P. Xiao, W. Shi, M. Xu and J. Peng, *IEEE Electr. Device Lett.*, 2012, **33**, 827.

12 P. Xiao, L. Lan, T. Dong, Z. Lin, W. Shi, R. Yao, X. Zhu and J. Peng, *Appl. Phys. Lett.*, 2014, **104**, 51607.

13 G. Adamopoulos, S. Thomas, P. H. Wöbkenberg, D. D. C. Bradley, M. A. McLachlan and T. D. Anthopoulos, *Adv. Mater.*, 2011, **23**, 1894.

14 B. S. Ong, C. Li, Y. Li, Y. Wu and R. Loutfy, *J. Am. Chem. Soc.*, 2007, **129**, 2750.

15 Y. Jung, W. Yang, C. Y. Koo, K. Song and J. Moon, *J. Mater. Chem.*, 2012, **22**, 5390.

16 H. Wang, T. Sun, W. Xu, F. Xie, L. Ye, Y. Xiao, Y. Wang, J. Chen and J. Xu, *RSC Adv.*, 2014, **4**, 54729.

17 J. Jang, R. Kitsomboonloha, S. L. Swisher, E. S. Park, H. Kang and V. Subramanian, *Adv. Mater.*, 2013, **25**, 1042.

18 B. Zhang, H. Li, X. Zhang, Y. Luo, Q. Wang and A. Song, *Appl. Phys. Lett.*, 2015, **106**, 93506.

19 J. Yoon, Y. H. Kim, J. Ka, S. Hong, M. H. Yi and K. Jang, *J. Mater. Chem. C*, 2014, **2**, 2191.

20 T. Pan, C. Chen and J. Liu, *RSC Adv.*, 2014, **4**, 29300.

21 L. J. Li, H. Deng, L. P. Dai, J. J. Chen, Q. L. Yuan and Y. Li, *Mater. Res. Bull.*, 2008, **43**, 1456.

22 D. N. Kim, D. L. Kim, G. H. Kim, S. J. Kim, Y. S. Rim, W. H. Jeong and H. J. Kim, *Appl. Phys. Lett.*, 2010, **97**, 192105.

23 C. Lee, Y. Lin and J. Lin, *J. Appl. Phys.*, 2015, **117**, 45309.

24 B. M. Reddy, P. Bharali, P. Saikia, A. Khan, S. Loridant, M. Muhler and W. Grunert, *J. Phys. Chem. C*, 2007, **111**, 1878.

25 Y. Jeong, C. Bae, D. Kim, K. Song, K. Woo, H. Shin, G. Cao and J. Moon, *ACS Appl. Mater. Interfaces*, 2010, **2**, 611.

26 G. H. Kim, H. S. Kim, H. S. Shin, B. D. Ahn, K. H. Kim and H. J. Kim, *Thin Solid Films*, 2009, **517**, 4007.

Figure & Table Captions

Table 1. The electrical parameters of IZO TFTs with the ZrO_x/AlO_x and AlO_x gate insulators

Fig. 1. (a) Schematic structure of the IZO-TFT with ZrO_x/AlO_x bilayer gate insulator. (b) Cross-sectional STEM image for IZO-TFT with ZrO_x/AlO_x gate insulator. (c) HR-TEM image of $IZO/ZrO_x/AlO_x$ cross-sectional structure. (d) FFT patterns obtained from Area 1-6.

Fig. 2. Typical output characteristics for IZO-TFTs with (a) ZrO_x/AlO_x gate insulator and (b) AlO_x gate insulator. (c) Typical transfer curves and the corresponding I_G versus V_G curves of IZO-TFTs with the ZrO_x/AlO_x and AlO_x gate insulator.

Fig. 3. HAADF STEM images together with the elemental distribution detected by EDS for (a) IZO/AlO_x region, and (b) $IZO/ZrO_x/AlO_x$ region.

Fig. 4. EDS line scan profiles collected from (a) IZO/AlO_x region, and (b) $IZO/ZrO_x/AlO_x$ region.

Fig. 5. XPS spectra of the O 1s core level line for the IZO films with different substrates of (a) AlO_x layer and (b) ZrO_x/AlO_x layer. (c) O 1s XPS spectrum collected from AlO_x layer. (d) Al 2p XPS spectra collected from different samples. (e) In 3d XPS spectra collected from IZO film deposited on ZrO_x/AlO_x layer and AlO_x layer.

Table 1

Table 1 The electrical parameters of IZO TFTs with the ZrO_x/AlO_x and AlO_x gate insulators

Insulator	Mobility ($cm^2\ V^{-1}\ s^{-1}$)	V_{th} (V)	I_{on}/I_{off}	*SS* (V/dec)
Without ZrO_x	2.8	4.9	4.8×10^6	0.33
With ZrO_x	7.8	4.6	3.5×10^6	0.21

Figure 1

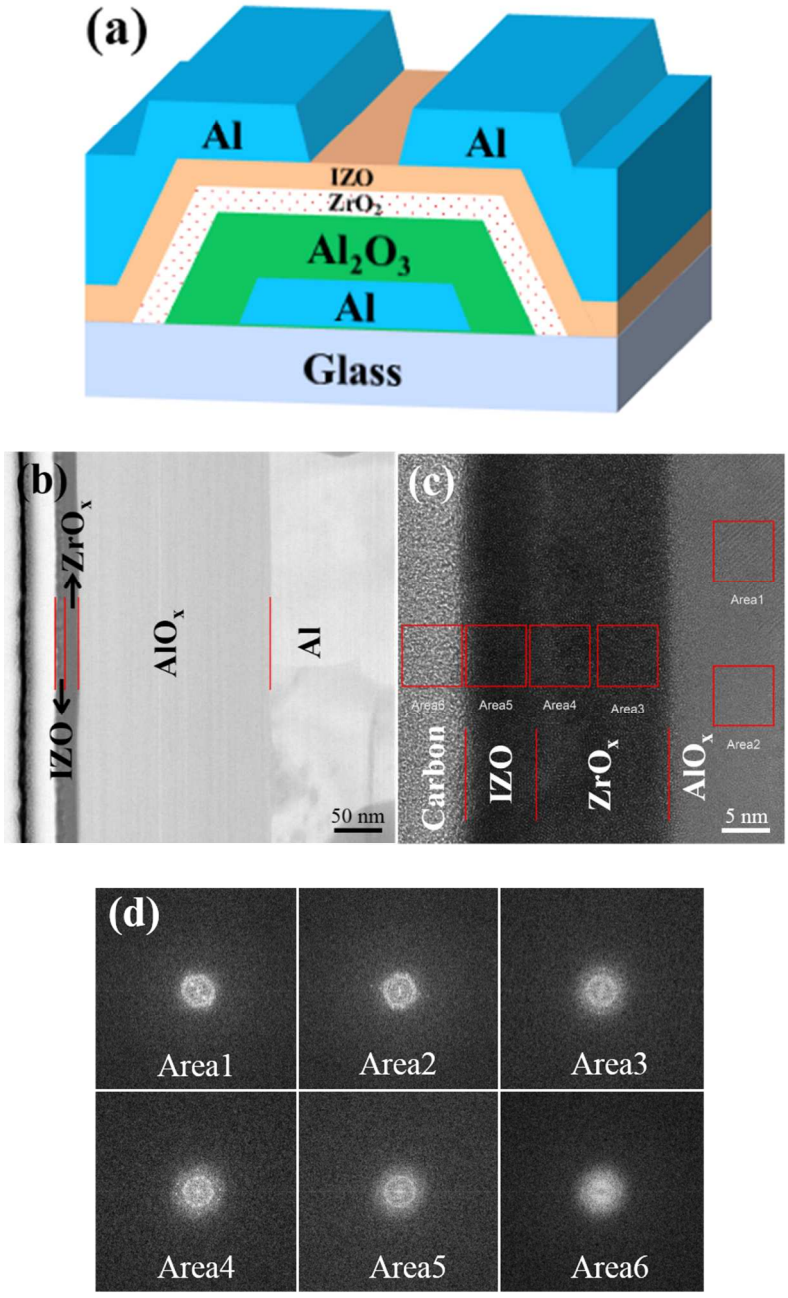

Fig. 1 (a) Schematic structure of the IZO-TFT with ZrO_x/AlO_x bilayer gate insulator. (b) Cross-sectional STEM image for IZO-TFT with ZrO_x/AlO_x gate insulator. (c) HR-TEM image of $IZO/ZrO_x/AlO_x$ cross-sectional structure. (d) FFT patterns obtained from Area 1-6.

Figure 2

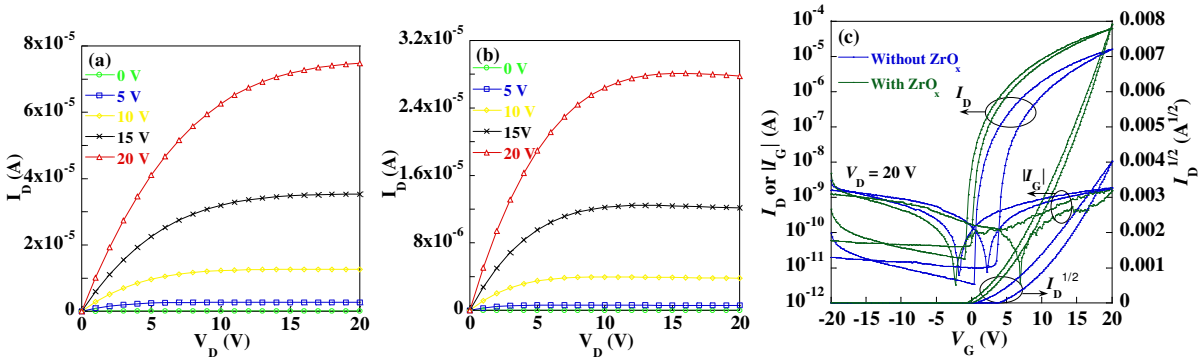

Fig. 2 Typical output characteristics for IZO-TFTs with (a) ZrO_x/AlO_x gate insulator and (b) AlO_x gate insulator. (c) Typical transfer curves and the corresponding I_G versus V_G curves of IZO-TFTs with the ZrO_x/AlO_x and AlO_x gate insulator.

Figure 3

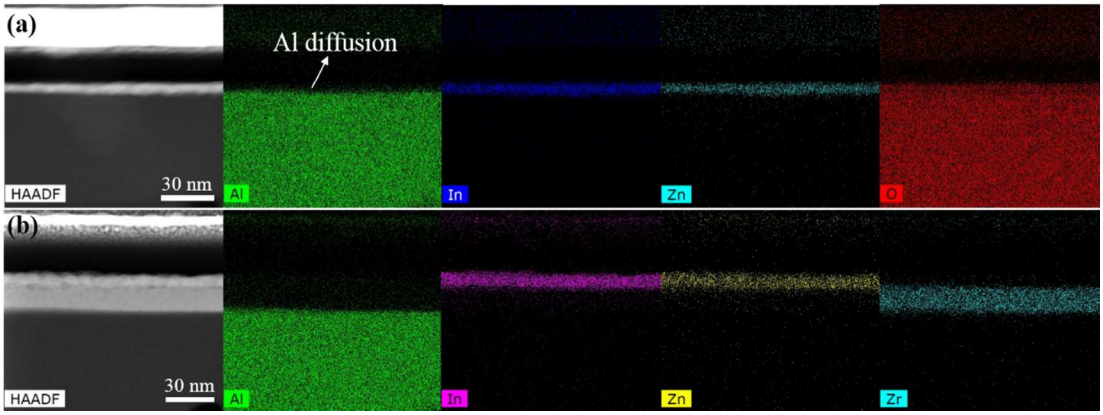

Fig. 3 HAADF STEM images together with the elemental distribution detected by EDS for (a) IZO/AlO_x region, and (b) IZO/ZrO_x/AlO_x region.

Figure 4

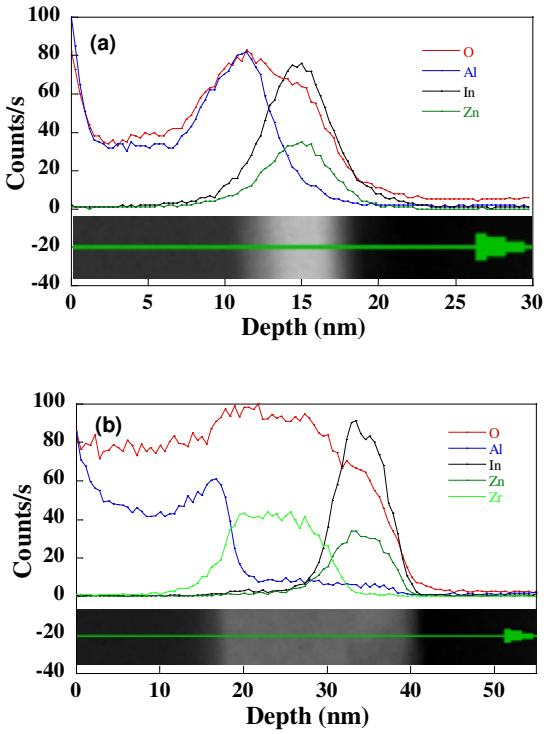

Fig. 4 EDS line scan profiles collected from (a) IZO/AlO_x region, and (b) IZO/ZrO_x/AlO_x region.

Figure 5

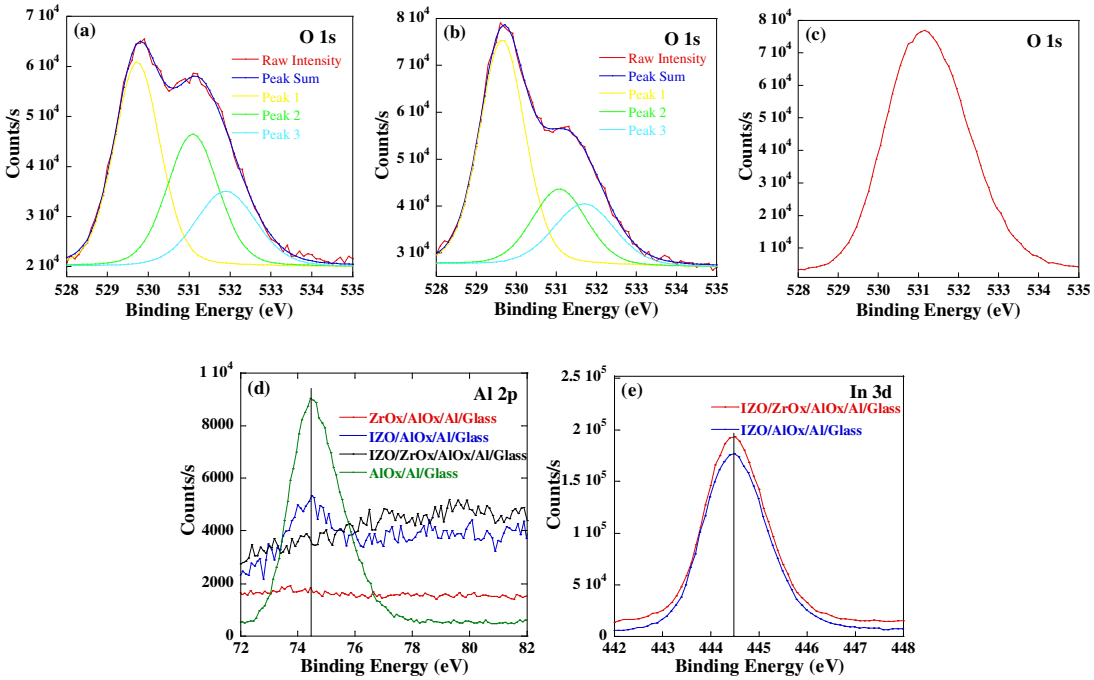

Fig. 5 XPS spectra of the O 1s core level line for the IZO films with different substrates of (a) AlO_x layer and (b) ZrO_x/AlO_x layer. (c) O 1s XPS spectrum collected from AlO_x layer. (d) Al 2p XPS spectra collected from different samples. (e) In 3d XPS spectra collected from IZO film deposited on ZrO_x/AlO_x layer and AlO_x layer